Nanoscale elastic-property measurements and mapping using atomic force acoustic microscopy methods*

D C Hurley, M Kopycinska-Müller, A B Kos and R H Geiss

National Institute of Standards & Technology, Boulder, CO 80305-3328, USA

E-mail: hurley@boulder.nist.gov

Abstract
We describe a dynamic atomic force microscopy (AFM) method for
measuring the elastic properties of surfaces, thin films and nanostructures at
the nanoscale. Our approach is based on atomic force acoustic microscopy
(AFAM) techniques and involves the resonant modes of the AFM cantilever
in contact mode. From the frequencies of the resonant modes, the tip–
sample contact stiffness k^* can be calculated. Values for elastic properties
such as the indentation modulus M can be determined from k^* with
appropriate contact-mechanics models. We present the basic principles of
AFAM and explain how it can be used to measure local elastic properties
with a lateral spatial resolution of tens of nanometres. Quantitative results
for a variety of films as thin as 50 nm are given to illustrate our methods.
Studies related to measurement accuracy involving the effects of film
thickness and tip wear are also described. Finally, we discuss the design and
use of electronics to track the contact-resonance frequency. This extension
of AFAM fixed-position methods will enable rapid quantitative imaging of
nanoscale elastic properties.

Keywords: elastic properties, atomic force microscopy, atomic force acoustic
microscopy, nanomechanics

1. Introduction

As critical dimensions in industrial and technological
applications shrink below 1 μm, new tools are required to
investigate material properties on commensurate scales. In
particular, nanomechanical information—knowledge on the
nanometre scale of mechanical properties such as elastic
modulus, strength, adhesion and friction—is needed in
many emerging products. The need is driven by the
increasing integration of multiple materials, sometimes with
very different properties, on micro- and nanometre scales.
The complexity of such systems increases the demand for
accurate property values, so that predictive modelling of
mechanical reliability can be performed. Furthermore,
because the cause of failure is often a localized variation in
properties, measurements of 'average' sample properties are
not necessarily sufficient. Instead, quantitative images of the
spatial distribution in properties are increasingly demanded.

One approach to meet this objective combines
nanoindentation techniques [1] with force modulation and
scanning [2]. This promising method is limited in lateral
spatial resolution by the radius (a few hundred nanometres)
of the Berkovich diamond indenter used. Therefore, methods
that exploit the increased spatial resolution of atomic force
microscopy (AFM) are also being developed. AFM methods
that promise quantitative information are usually dynamic
approaches in which the AFM cantilever is vibrated at or near
the frequencies of its resonant modes. Two of these approaches
are contact methods called atomic force acoustic microscopy
(AFAM) [3–6] and ultrasonic AFM [7–10].

Here we describe our progress towards quantitative
measurement and imaging of nanoscale elastic properties
with AFAM. We first summarize the basic experimental
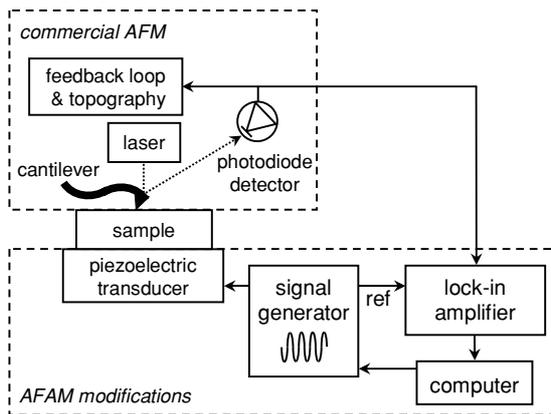
Figure 1. Schematic of experimental AFAM apparatus used for modulus measurements at a fixed sample position.

Figure 2. Comparison between AFAM and nanoindentation results. Shown are values for the indentation modulus M obtained on different supported thin films: niobium (Nb), nickel (Ni), aluminium (Al), hydrogenated silicon carbide (SiC:H) and fluorinated silica glass (FSG). The thickness t of each film is indicated.

and theoretical concepts of AFAM. Next, we present our results for the elastic modulus of several supported thin films using fixed-position AFAM techniques. Studies to investigate measurement accuracy involving the effects of tip wear and film thickness are also discussed. Finally, we describe our work to extend AFAM methods for achieving rapid imaging of contact-resonance frequencies. From such frequency images, quantitative images or maps of elastic properties may ultimately be determined.

2. Modulus measurements at a fixed position

2.1. Techniques and methods

Detailed descriptions of the experimental and theoretical methods for determining elastic properties with AFAM are available elsewhere [3, 4]. Here we give only a brief summary. A schematic of the experimental apparatus is shown in figure 1. A function generator drives a piezoelectric transducer with a continuous sine wave (frequency ~0.1–3.5 MHz, amplitude ~25–500 mV). When the tip of the AFM cantilever is in contact with the sample and the transducer vibrations have the appropriate frequency, resonant modes of the cantilever are excited. The amplitude of cantilever vibration at the transducer excitation frequency is detected from the AFM photodiode signal by use of a lock-in amplifier.

By sweeping the excitation frequency, a spectrum of the cantilever response versus frequency can be acquired. The frequencies of the cantilever's first two flexural resonant modes (the 'contact-resonance frequencies') are determined from such spectra. AFAM experiments require the use of a reference material with known elastic properties. Measurements are made on the reference material in alternation with those on the unknown (test) material. This approach avoids direct measurement of the contact radius, which is difficult to determine in practice. Two sets of results are obtained: one for the test data relative to the first reference data and one for the test data relative to the second reference data. The two data sets are averaged to obtain a single value for the modulus in order to minimize the effects of tip wear.

The experimental spectra are typically interpreted with an analytical model for the cantilever beam dynamics [3]. The beam-dynamics model provides a characteristic equation that links the measured frequencies to the tip–sample contact stiffness k^*. From k^* and knowledge of the reference material's properties, first the reduced Young's modulus E^* and then the indentation modulus M_{test} can be calculated [11]:

$$E_{test}^* = E_{ref}^* \left(\frac{k_{test}^*}{k_{ref}^*} \right)^n, \tag{1}$$

$$\frac{1}{E_{test}^*} = \frac{1}{M_{tip}} + \frac{1}{M_{test}}, \tag{2}$$

where the subscript 'test' indicates the unknown sample and 'ref' refers to the reference sample. M_{tip} is the indentation modulus of the $\langle 1\,0\,0 \rangle$ silicon tip (165 GPa). For isotropic materials $M = E/(1 - \nu^2)$, where E is Young's modulus and ν is Poisson's ratio. The value of n in equation (1) depends on the contact-mechanics model used [12]. Here we cite values of M calculated using $n = 3/2$, which corresponds to Hertzian contact between a hemispherical indenter and a halfspace.

For an AFM tip located at the exact end of the cantilever, the values for k^* obtained from the different contact-resonance frequencies are usually not equal. Therefore, the characteristic equation for sample-coupled vibration has been modified to account for other tip positions [3]. In this case, k^* is calculated as a function of tip position for each of the two flexural modes. The two values of k^* at each tip position are compared, and the position at which k^* is the same for the two modes is taken as the solution. Thus the effective tip position can be considered an adjustable parameter for data analysis. Typical values of the tip position are between 0.91 and 0.98 times the length of the cantilever. These values roughly agree with scanning electron microscopy (SEM) measurements of actual cantilever dimensions [4].

2.2. Comparison with nanoindentation

To test the accuracy of our methods, we compared AFAM values for the indentation modulus M to those obtained by another contact-probe technique, depth-sensing indentation (commonly known as nanoindentation) [1]. Measurements were performed by both methods on several samples consisting of blanket films attached to substrates. The films, which comprised a variety of materials as indicated in figure 2, were usually deposited on silicon wafer substrates with sputtering

Table 1. Results for three nanocrystalline nickel thin-film samples: film thickness t, average grain diameter d and indentation modulus M_{AFAM} measured with AFAM. Values of the volume fraction V_{ic} of intercrystalline material and the corresponding modulus M_{nc} for a nanocrystalline, composite material were estimated from d using literature models. The error bars for t, d and M_{AFAM} represent one standard deviation in uncertainty based on scatter in the individual measurements. The error bars for V_{ic} and M_{ic} were calculated from the uncertainty in d.

t (nm)	d (nm)	V_{ic} (%)	M_{nc} (GPa)	M_{AFAM} (GPa)
772 ± 5	23 ± 8	12 ± 4	230 ± 7	223 ± 28
204 ± 4	20 ± 6	14 ± 4	226 ± 7	220 ± 19
53 ± 2	11 ± 3	25 ± 6	208 ± 10	210 ± 26

methods. The film thickness was measured by a stylus profilometer or by analysis of the sample in cross section with SEM. In each case, AFAM and nanoindentation measurements were performed on different sections of the same sample. The nanoindentation experiments were performed by our collaborators (see acknowledgments).

Figure 2 gives the AFAM and nanoindentation values for M as well as the film thickness t for each sample. It can be seen that the films possessed a fairly wide range of stiffness ($\sim$50–250 GPa) and thickness ($\sim$0.3–3 μm) values. The figure shows that the AFAM and nanoindentation results are in very good agreement (differences of less than 10% and within the measurement uncertainty) for all the samples. Furthermore, the absolute values for M agree with values available in the literature for the corresponding bulk materials. (The only exception is the nickel film, which will be discussed further in the next section.) These results give us confidence in the validity of our quantitative methods.

2.3. Investigation of film thickness effects

Analysis of nanoindentation data on thin-film samples is often complicated by the fact that the mechanical properties of the substrate affect the measured values. The thickness at which these effects become significant depends on the elastic properties of both the film and the substrate, but a thickness of approximately 1 μm is usually given as a rough guideline. To obtain accurate nanoindentation results on thin-film samples, therefore, complex calibration and analysis procedures may be needed. AFAM measurements on thin films may also contain substrate effects, but the thickness at which they become significant should be much lower due to the smaller contact radius and applied forces. To investigate how film thickness affects AFAM measurements of elastic properties, we performed experiments on a series of nickel films. The films were deposited by DC magnetron sputtering techniques on (0 0 1) silicon substrates and had nominal thickness values of 800 nm, 200 nm and 50 nm. Analysis with SEM and x-ray diffraction (XRD) indicated that the films were nanocrystalline with a strong (1 1 1) fibre texture.

Table 1 shows our results for the three nickel film samples. For comparison, literature values of the indentation modulus M for single-crystal nickel range from approximately 220 GPa in the $\langle 1\,0\,0 \rangle$ direction to 250 GPa in the $\langle 1\,1\,1 \rangle$ direction. It can be seen that the AFAM values of M for the thin-film samples were lower than expected for $\langle 1\,1\,1 \rangle$-textured nickel. Because

the (0 0 1) silicon substrate is more compliant than the nickel film ($M = 165$ GPa), substrate effects are a potential source of the observed reduction in stiffness. To investigate this issue, we estimated the values of stress and deformation at the sample surface and at the film–substrate interface [13]. The values were calculated using equations for the stress distribution in the sample as a function of the stress applied at the surface assuming Hertzian contact mechanics [14]. If the stress and deformation in the substrate at the film–substrate interface are negligible compared to their values directly under the tip, then substrate effects can be safely ignored. For the film approximately 800 nm thick, the substrate deformation at the film–substrate interface was about 0.1% of its value at the tip, while the stress at the interface was less than 0.03% of its value directly under the tip. For the thinnest film, which was approximately 50 nm thick, the estimated stress amplitude at the interface ranged from 3 to 6% of its value under the tip, depending on the experimental conditions. The corresponding deformation in the substrate at the film–substrate interface was about 4 to 8% of its value under the tip. We consider these stresses and strains to be insignificant. These results indicate that AFAM methods can be used to directly measure the modulus of even nanothin films ($t < 100$ nm), without having to consider substrate effects. The film thickness for which the substrate begins to play a role depends on the elastic properties of both the tip and the sample.

Although these conclusions about film thickness effects (or lack thereof) have significant implications for AFAM experiments, it means that thickness effects are probably not the reason for the reduced values of modulus measured in the nickel films. A more likely explanation is that nanocrystalline effects cause the observed reduction in modulus. Nanocrystalline films contain an increased volume fraction of intercrystalline components (grain boundaries and triple junctions) with reduced elastic modulus [15]. Using literature models for nanocrystalline materials [15] and values of the average grain diameter measured by SEM given in table 1, we estimated the volume fraction V_{ic} of intercrystalline material in each film. We assumed that the modulus of the intercrystalline material was 0.32 times that of the crystalline phase (250 GPa) [16]. From these modulus values and the values of V_{ic}, we calculated the effective modulus M_{nc} of the composite materials using a rule-of-mixtures weighting [16]. The values for M_{nc} obtained in this way are shown in table 1. The values agree with the values M_{AFAM} obtained by AFAM within the measurement uncertainty. Therefore, we believe that the measured reduction in modulus can be attributed to nanocrystalline effects.

2.4. Tip wear studies

Studies such as those described above demonstrate the validity of our basic approach. However, the quantitative accuracy and reliability of AFAM could be improved by refining various aspects of the technique. In particular, we seek to improve our understanding and control of the actual tip–sample contact mechanics. AFAM contact-resonance frequencies depend not only on elastic properties, but also on the value of the tip radius R. However, because current AFAM methods involve scanning the silicon AFM tip across a material of roughly

Figure 3. SEM images of an AFM tip (*a*) before use and (*b*)–(*d*) after repeated use in AFAM experiments. (*a*) The radius of curvature R is < 10 nm. (*b*) The tip end has broken and $R = 19 \pm 2$ nm. Further increase in R as well as the width of the tip can be seen in (*c*) ($R = 21 \pm 4$ nm) and (*d*) ($R = 37 \pm 2$ nm).

equivalent stiffness, tip damage is inevitable and R can change significantly. Thus knowledge of R and how it changes over time is essential for accurate measurements of elastic properties with AFAM and other contact AFM methods.

To address the issue of tip wear and its influence on AFAM measurements of elastic properties, we performed a series of experiments combining AFAM measurements and direct tip visualization with SEM. AFAM measurements were performed with several different cantilevers on a sample with known elastic properties (fused quartz). From the experimental values of the tip–sample contact stiffness k^*, values for the tip radius R were calculated assuming both Hertzian and Derjaguin–Müller–Toporov (DMT) contact mechanics [12]. Independent values for R before and after each sequence of AFAM measurements were obtained from high-resolution SEM images. Figure 3 shows a series of such SEM images for one tip used in this study. Both the AFAM results and the SEM images indicated that R increased with use. However, the values of R predicted by either contact-mechanics model from the AFAM data were consistently smaller than the SEM (actual) values. In addition, in some cases the AFAM results suggested a hemispherical tip, while the corresponding SEM images showed that the end of the tip was flat. Other changes in tip shape were occasionally observed, for instance an increase in tip width. Further experiments are planned to study these effects in more detail. Knowledge gained in this way will eventually allow us to control the experimental contact mechanics and thus lead to improved measurement accuracy and repeatability, particularly in imaging applications.

3. Quantitative stiffness imaging

3.1. Experimental methods

As explained above, we ultimately desire *nanomechanical mapping*—that is, quantitative imaging of nanoscale elastic properties. Directly combining the single-point AFAM methods described above with two-dimensional scanning is not practical, because lock-in techniques are typically much too slow—requiring perhaps as many as several days for a single image [9]. This problem has previously been addressed by other groups [5, 6, 9, 10]. Our approach to overcoming this difficulty involves new signal acquisition and processing methods based on a 32-bit floating-point digital signal processor (DSP). A block diagram of the circuit is shown in figure 4. Briefly, the circuit applies an

Figure 4. Schematic diagram of experimental AFAM apparatus for resonant-frequency imaging.

adjustable-amplitude, swept-frequency sinusoidal voltage to the piezoelectric transducer under the sample. A wideband, root-mean-square-to-DC (RMS-to-DC) converter fed by a low-noise operational amplifier with a noninverting gain of 100 is used to detect the magnitude of the photodiode signal and deliver it to an analogue-to-digital converter. The RMS-to-DC converter has a linear response from approximately 1 kHz to 3.2 MHz. From the RMS voltage response as the frequency is swept, the circuit constructs a complete resonance curve and finds its peak. This information is sent to a digital feedback control loop that adjusts a voltage-controlled oscillator (VCO) to tune the centre frequency of vibration. In this way, the sweep window remains centred on the cantilever resonance. The control voltage is also sent to the AFM's auxiliary image input port. Thus each pixel in the acquired image contains a value proportional to the peak (i.e., resonant) frequency at that position. A frequency range can be specified in order to exclude all but the cantilever mode of interest.

Some of the most important features of the DSP circuit include an enhanced direct memory access (DMA) controller that enables data acquisition independent of the DSP core, a multichannel buffered serial port to communicate with the analogue-to-digital (A/D) and digital-to-analogue (D/A) converters, and a multi-unit processor core capable of 600 million floating point operations per second. The 20-bit delta-sigma A/D and D/A converters are located on a stereo audio daughtercard mated to the DSP board and operate at 48 kilosamples per second. At 48 kilosamples per second and 128 samples per spectrum, the system is capable of acquiring the full cantilever resonance spectrum every 2.7 ms (375 Hz repetition rate). In its current form, the circuit realizes approximately 17–18 bits of resolution, corresponding to an intrinsic frequency resolution of $\sim$12 Hz over a full-range span of 3 kHz to 3 MHz.

3.2. Results and discussion

Figure 5 shows results obtained using the frequency-tracking methods described above. The sample consisted of a stack of two thin films deposited on a silicon wafer. The top film was a niobium (Nb) 'wire' approximately 200 nm thick and 4 μm

Figure 5. Results of resonant-frequency imaging experiments. Contact-resonance frequency images of (*a*) the first flexural mode f_1 and (*b*) the second flexural mode f_2 for a Nb/SiO$_2$ sample. (*c*) Corresponding image for the normalized vertical contact stiffness k^*/k_c calculated from the frequency images in (*a*) and (*b*). (*d*) Corresponding image of the indentation modulus M calculated from (*c*), assuming Hertzian contact mechanics.

wide. The Nb film was sputtered on top of a blanket film of silica (SiO$_2$) approximately 350 nm thick created by plasma-enhanced chemical vapour deposition. Quantitative fixed-point AFAM experiments were performed to independently determine the elastic properties of the constituent films. Using a reference sample of fused silica ($M_{ref} = 74.9$ GPa), we obtained $M_{SiO_2} = 75.1 \pm 10.0$ GPa for the SiO$_2$ film and $M_{Nb} = 112.7 \pm 15.0$ GPa for the Nb film. These values represent the averages and standard deviations of more than 20 individual measurements for each film. These results fall within the range of literature values for bulk fused silica $\left(M_{SiO_2} \approx 72\text{–}77\,\text{GPa}\right)$ and bulk Nb ($M_{Nb} \approx 116\text{–}133$ GPa).

For data acquisition, we used a silicon cantilever with a nominal cantilever spring constant $k_c = 47$ N m^{-1} provided by the vendor. The measured free-space resonant frequencies of the first two flexural modes were 167.55 and 1044.0 kHz. Contact-resonance frequency images for the Nb/SiO$_2$ sample with this cantilever are shown in figures 5(*a*) and (*b*) for the first (f_1) and second (f_2) flexural modes, respectively. The central Nb stripe stands out clearly in contrast to the left and right regions of SiO$_2$ film. The narrow, bright and dark vertical lines indicate relatively large frequency changes that occur at the interfaces between the SiO$_2$ and Nb films. Presumably, these are topographically induced frequency shifts caused by transient changes in the contact area as the tip moves from one material to another. The values of f_1 and f_2 for the individual materials are reasonably uniform and repeatable from line to line. The images also show that both f_1 and f_2 are greater

for the Nb film, suggesting that the contact stiffness is greater here. This hypothesis is verified in figure 5(*c*), which contains a map of the normalized contact stiffness k^*/k_c obtained from figures 5(*a*) and (*b*). Figure 5(*c*) was calculated on a pixel-by-pixel basis using the single-point AFAM methods described above.

Although contact-stiffness images are useful for visualizing relative property distributions, maps of the sample's elastic properties are preferred. We found experimentally that the tip–sample contact for a moving tip differed from that of a static contact. Therefore, instead of comparing the values of k^*/k_c in figure 5(*c*) to those from point measurements of a reference sample, we applied a 'self-calibrating' approach. We assumed that the mean value of k^*/k_c for the SiO$_2$ region corresponded to the previously measured value of $M_{SiO_2} = 75.1$ GPa. With this assumption and using the Hertzian contact model, values of M for the entire image were calculated. The corresponding image, shown in figure 5(*d*), indicates that the values obtained are physically reasonable. The mean value for the entire region of SiO$_2$ film is $M_{SiO_2} = 75.5 \pm 7.1$ GPa, while the mean value for the Nb film region is $M_{Nb} = 118.5 \pm 7.1$ GPa. This is in good agreement with both the fixed-point value of 112.7 ± 15.0 GPa obtained above and with literature values of 116 to 133 GPa for Nb. Both of these results were calculated from image regions containing more than 2×10^4 pixels. Furthermore, the relatively small (5–10%) standard deviation of the results indicates that the tip–sample contact is fairly consistent and repeatable for a given material.

With our specific circuit components, the frequency-tracking electronics perform a frequency sweep approximately every 2.7 ms (repetition rate 375 Hz). The AFM acquisition speed (scan speed) must be adjusted so that several sweeps are performed at each image position. The scan size and contrast in elastic properties (i.e., the relative frequency shift) also affect the acquisition rate. We found that for scans a few to several micrometres in size, it was usually sufficient to operate at a scan rate of 0.2 Hz (5 s/line) when acquiring images 256 pixels wide. At a scan rate of 0.2 Hz, a 256×256 image requires ~22 min. Thus, it takes less than 1 h to acquire frequency images for two resonant modes.

As currently implemented, our electronics can track only one contact-resonance frequency at a time. Current AFAM analysis methods require frequency information from two modes to calculate contact-stiffness values. Thus it is necessary to image the sample twice in order to obtain accurate modulus maps. This approach is less than optimal due to potential spatial drift from one image to the next. Furthermore, extended scanning could result in tip wear; any resulting increase in tip radius would increase the measured contact-resonance frequencies. Tip wear was minimized in our experiments by using relatively low applied forces. Analysis of regions near the top and bottom of the images (i.e., the beginning and end of a scan) indicated little, if any, difference in the measured frequencies. Imaging two contact-resonance frequencies during the same scan would greatly reduce the effects of drift and wear. The DSP architecture of the electronics lends itself to such changes in implementation because changes are made in software instead of hardware. Thus dual-frequency imaging may be possible in the future.

4. Summary and conclusions

We have described our work to quantitatively measure nanoscale elastic properties using dynamic AFM methods. Our approach is based on AFAM, a contact technique involving resonant modes of the AFM cantilever. We have shown how AFAM methods can be used to measure the indentation modulus of a variety of thin films. The AFAM results were in good agreement with results from more conventional techniques such as nanoindentation. AFAM successfully measured films as thin as 50 nm, which present major measurement challenges for nanoindentation. SEM imaging studies to investigate the actual tip geometry and how it changes with time were also described. Finally, we have discussed techniques that combine quantitative point methods with AFM scanning capabilities to achieve nanoscale elastic-property mapping. Frequency-tracking electronics have been developed to rapidly image the contact-resonance frequency in a given region of the sample surface. From the flexural frequency images, maps of the contact stiffness and the indentation modulus can be obtained. Although these results are promising, achieving the goal of quantitative modulus mapping requires further effort to understand and control such issues as surface topography, tip wear and the actual tip–sample contact behaviour.

Acknowledgments

References

[1] Oliver W C and Pharr G M 1992 An improved technique for determining hardness and elastic modulus using load and displacement sensing indentation experiments *J. Mater. Res.* **7** 1564

[2] Syed Asif S A, Wahl K J, Colton R J and Warren O L 2001 Quantitative imaging of nanoscale mechanical properties using hybrid nanoindentation and force modulation *J. Appl. Phys.* **90** 1192

[3] Rabe U, Amelio S, Kester E, Scherer V, Hirsekorn S and Arnold W 2000 Quantitative determination of contact stiffness using atomic force acoustic microscopy *Ultrasonics* **38** 430

[4] Hurley D C, Shen K, Jennett N M and Turner J A 2003 Atomic force acoustic microscopy methods to determine thin-film elastic properties *J. Appl. Phys.* **94** 2347

[5] Rabe U, Kopycinska M, Hirsekorn S, Muñoz Saldaña J, Schneider G A and Arnold W 2002 High-resolution characterization of piezoelectric ceramics by ultrasonic scanning force acoustic microscopy techniques *J. Phys. D: Appl. Phys.* **35** 2621

[6] Efimov E and Saunin S A 2002 Atomic force acoustic microscopy as a tool for polymer elasticity analysis *Proc. Scanning Probe Microscopy Conf. (Nizhny Novgorod)* p 79 http://www.nanoworld.org/english/SPM2002/contents.htm (accessed January 2005)

[7] Yamanaka K, Noguchi A, Tsuji T, Koike T and Goto T 1999 Quantitative material characterization by ultrasonic AFM *Surf. Interface Anal.* **27** 600

[8] Geer R E, Kolosov O V, Briggs G A D and Shekhawat G S 2002 Nanometer-scale mechanical imaging of aluminum damascene interconnect structures in a low-dielectric-constant polymer *J. Appl. Phys.* **91** 4549

[9] Yamanaka K, Maruyama Y, Tsuji T and Nakamoto K 2001 Resonance frequency and Q factor mapping by ultrasonic atomic force acoustic microscopy *Appl. Phys. Lett.* **78** 1939

[10] Kobayashi K, Yamada H and Matsushige K 2002 Resonance tracking ultrasonic atomic force microscopy *Surf. Interface Anal.* **33** 89

[11] Rabe U, Amelio S, Kopycinska M, Hirsekorn S, Kempf M, Göken M and Arnold W 2002 Imaging and measurement of local mechanical material properties by atomic force acoustic microscopy *Surf. Interface Anal.* **33** 65

[12] Maugis D 1992 Adhesion of spheres: the JKR-DMT transition using a Dugdale model *J. Colloid Interface Sci.* **150** 243

[13] Kopycinska-Müller M, Geiss R H, Müller J and Hurley D C 2005 Elastic-property measurements of ultrathin films using atomic force acoustic microscopy *Nanotechnology* **16** 703

[14] Johnson K L 1985 *Contact Mechanics* (Cambridge: Cambridge University Press)

[15] Palumbo G, Thorpe S J and Aust K T 1990 On the contribution of triple junctions to the structure and properties of nanocrystalline materials *Scr. Metall. Mater.* **24** 1347

[16] Wang G-F, Feng X-Q, Yu S-W and Nan C-W 2003 Interface effects on effective elastic moduli of nanocrystalline materials *Mater. Sci. Eng.* A **363** 1